AGU PUBLICATIONS

Geochemistry, Geophysics, Geosystems

RESEARCH ARTICLE
10.1002/2015GC006093

Frictional properties of gabbro at conditions corresponding to slow slip events in subduction zones

E. K. Mitchell[1], Y. Fialko[1], and K. M. Brown[1]

[1]Institute of Geophysics and Planetary Physics, Scripps Institution of Oceanography, University of California, San Diego, San Diego, California, USA

Key Points:
- Frictional sliding of gabbro is velocity weakening at temperatures up to 600°C
- Occurrence of SSEs in subduction zones cannot be explained by temperature-dependent gabbro friction
- Presence of clay minerals, transformation to greenschist facies may govern slow slip events

Correspondence to:
E. K. Mitchell,
ekmitche@ucsd.edu

Citation:
Mitchell, E. K., Y. Fialko, and K. M. Brown (2015), Frictional properties of gabbro at conditions corresponding to slow slip events in subduction zones, *Geochem. Geophys. Geosyst.*, *16*, 4006–4020, doi:10.1002/2015GC006093.

Received 9 SEP 2015
Accepted 26 OCT 2015
Accepted article online 29 OCT 2015
Published online 26 NOV 2015

Abstract We conducted a series of experiments to explore the rate and state frictional properties of gabbro at conditions thought to be representative of slow slip events (SSEs) in subduction zones. The experiments were conducted using a heated direct shear apparatus. We tested both solid and simulated gouge samples at low effective normal stress (5–30 MPa) over a broad range of temperatures (20–600°C) under dry and hydrated conditions. In tests performed on dry solid samples, we observed stable sliding at low temperatures (20–150°C), stick slip at high temperatures (350–600°C), and a transitional "episodic slow slip" behavior at intermediate temperatures (200–300°C). In tests performed on dry gouge samples, we observed stable sliding at all temperatures. Under hydrated conditions, the gouge samples exhibited episodic slow slip and stick-slip behavior at temperatures between 300 and 500°C. Our results show a decrease in the rate parameter ($a - b$) with temperature for both solid and gouge samples; friction transitions from velocity strengthening to velocity weakening at temperature of about 150°C for both solid and gouge samples. We do not observe transition to velocity-strengthening friction at the high end of the tested temperature range. Our results suggest that the occurrence of slow slip events and the downdip limit of the seismogenic zone on subduction megathrusts cannot be solely explained by the temperature dependence of frictional properties of gabbro. Further experimental studies are needed to evaluate the effects of water fugacity and compositional heterogeneity (e.g., the presence of phyllosilicates) on frictional stability of subduction megathrusts.

1. Introduction

Over the last decade, geodetic observations revealed slow slip events (SSEs) in a number of subduction zones around the world [*Hirose et al*., 1999; *Dragert et al*., 2001; *Rogers and Dragert*, 2003; *Obara et al*., 2004; *Obara and Hirose*, 2006]. SSEs are characterized by accelerated fault creep at the bottom of the seismogenic zone that occurs over a time scale of the order of a few weeks, with a characteristic recurrence interval of the order of a year [*Dragert et al*., 2001; *Obara et al*., 2004]. Low-frequency earthquakes (LFEs), also known as nonvolcanic tremor, have been observed coincidentally with SSEs, and are thought to be the seismic signature of such events [*Obara*, 2002; *Rogers and Dragert*, 2003; *Ito et al*., 2007; *Bartlow et al*., 2011]. SSEs are thought to occur under conditions of very low effective normal stress, possibly due to locally elevated pore fluid pressure [*Matsubara et al*., 2009] in the transition zone between the velocity-weakening (seismogenic) and velocity-strengthening (aseismic) parts of the subduction megathrust [*Rubin*, 2008; *Liu and Rice*, 2009]. SSEs have been also reported in other tectonic environments [e.g., *Louie et al*., 1985; *Linde et al*., 1996; *Cervelli et al*., 2002; *Wei et al*., 2009], and used to argue for a continuum of slip modes ranging from stable creep to slow slip events to earthquakes [e.g., *Peng and Gomberg*, 2010].

Models of the earthquake cycle on subduction zone megathrusts are able to produce SSEs of reasonable size and duration by assuming low effective normal stress and rate-state friction parameters that have a temperature-dependent stability transition [*Liu and Rice*, 2005, 2009; *Rubin*, 2008; *Segall et al*., 2010]. For example, models of *Liu and Rice* [2009] assumed frictional parameters experimentally determined by *He et al*. [2007] for gabbro under hydrothermal conditions using a triaxial apparatus. As mentioned by *Liu and Rice* [2009], the experimental data are limited and ($a - b$) shows a dependence on loading conditions such as effective normal stress and load-point velocity, warranting more laboratory investigations at conditions corresponding to those at the inferred depths of SSEs. In this study, we investigate the frictional properties

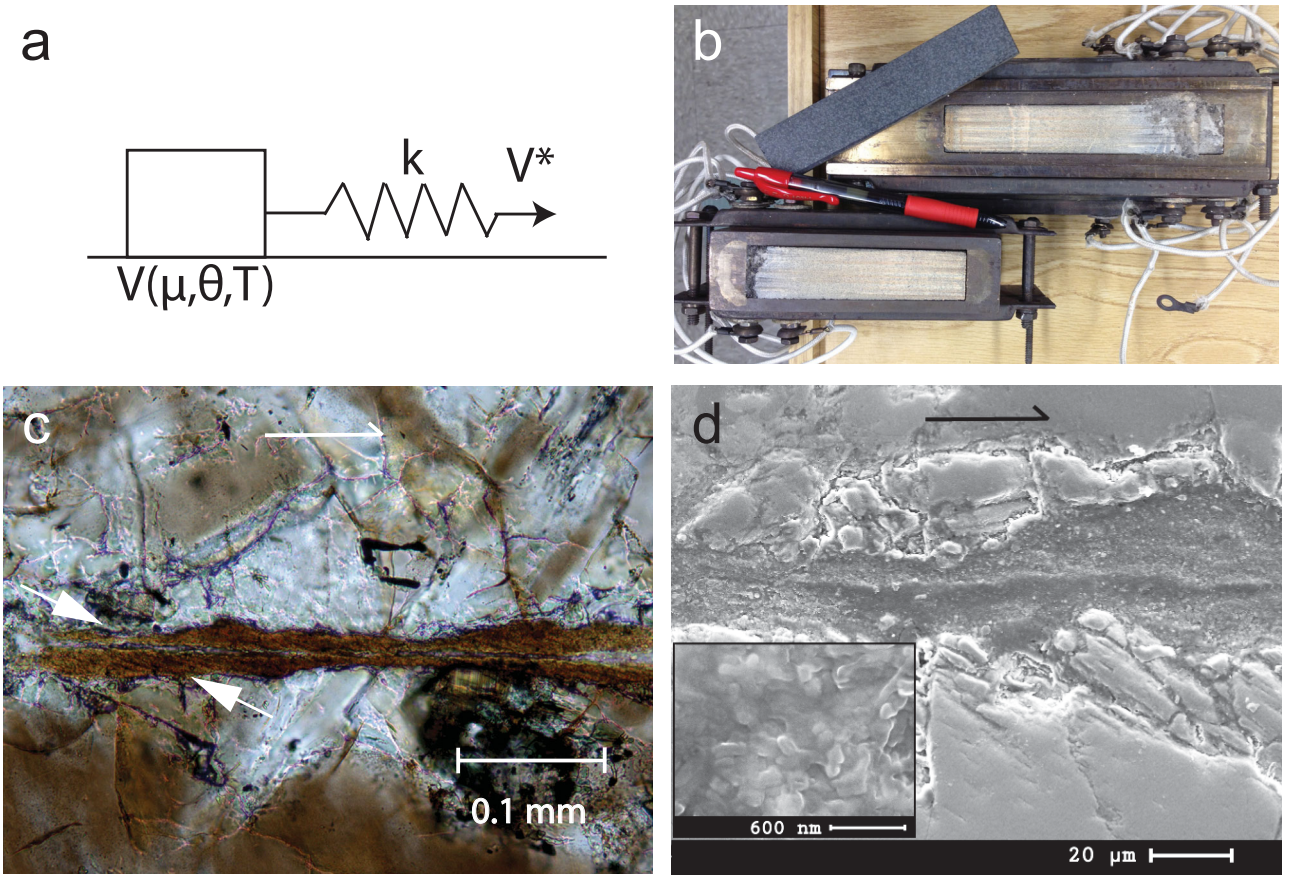

Figure 1. Experimental setup. (a) Diagram of 1-D spring-slider model. (b) Photograph of the gabbro samples after testing, with an intact sample for comparison and a pen for scale. (c) Microscope image of a portion of the shear zone after testing, under plane polarized transmitted light. Note the brown, very fine grained gouge layer within the shear zone, with possible Riedel shears (pointed out by arrows), indicative of primarily brittle deformation. (d) Scanning electron microscope (SEM) image of a portion of the shear zone, showing crushed grains along the shear surfaces and a layer of very small gouge particles. Inset figure is a close up of the gouge zone showing gouge particle size (of the order of hundreds of nanometers).

of gabbro under low normal stress, dry and hydrated conditions (low water fugacity), over a temperature range of 20–600°C. We find that slip becomes increasingly more unstable (velocity-weakening) with increasing temperature, up to the high-temperature limit of our experiments (600°C).

2. Experimental Setup

We conducted experiments using a heated direct shear apparatus in which rectangular blocks of gabbro with a total contact area of 2.64×10^3 mm^2 are contained in steel sample holders of matching geometry. The sample holders can also be used to test granular samples. Figure 1a is a diagram of a simple 1-D spring-slider model that closely approximates the experimental setup. Figure 1b shows the solid gabbro samples after testing, with an intact gabbro sample for comparison. The gabbro samples are composed of 63% plagioclase, 31% pyroxene, 3% magnetite, 2% olivine, and 1% chlorite. Average grain size is 0.5 mm. Solid samples were ground to a flatness of 4 μm/m and roughness of grit #80. Simulated gouge samples were created by crushing solid blocks of gabbro until they passed through a sieve with holes of diameter 1.67 mm. Gouge samples were initially 13 mm thick, and compacted to a thickness of 9 mm after being compressed to 30 MPa. The samples were "ran-in" by the initial slip of 160 mm at 5 MPa normal stress and room temperature. For solid samples, coefficient of friction evolved to a nearly constant value during the run-in, typically increasing from about 0.50 to 0.75 after total slip of about 100 mm, as a ~0.1 mm thick gouge layer accumulated between the rock surfaces. Displacements were measured using an LVDT transducer attached to the sample. Measured displacements included a small reversible component (0.03 mm/MPa for shear stress less than 15 MPa and 0.05 mm/MPa for shear stress greater than 15 MPa), most likely

resulting from tilting of the sample holder, as verified by cyclic increases and decreases in shear stress below the slip threshold. This reversible component was subtracted from the displacement data. We also removed any small linear trend in shear stress that was likely caused by irregularities along the slip interface. We heated the samples at 150°C for 30 min before all tests in order to reduce the effects of room humidity on dry tests performed at low temperatures. For more details about the experimental setup, see *Mitchell et al*. [2013]. To investigate the effects of water on frictional properties of the simulated gouge, we injected water at a rate of 0.02 mL/min into the bottom of the sample holder with a pressure cap of 0.7 MPa. Since the samples are unconfined, at temperatures above 100°C, the water flashes to vapor.

Experiments were conducted at normal stresses between 5 and 30 MPa, and load-point velocities between 10^{-6} and 3×10^{-2} mm/s. The tested range of normal stresses and slip velocities corresponds to conditions at the top and the bottom of the seismogenic zone on subduction megathrusts, where slow slip events occur. Effective normal stress at the bottom of the seismogenic zone is inferred to be very low (1–10 MPa) based on high V_p/V_s ratios [*Kodaira et al*., 2004; *Matsubara et al*., 2009], tremor triggered by Love waves [*Rubinstein et al*., 2007], aqueous metamorphic reactions in subducted rocks [*Dobson et al*., 2002; *Hacker et al*., 2003], and results of numerical simulations of the geodetically detected slow slip events [*Liu and Rice*, 2005, 2009; *Rubin*, 2008; *Segall et al*., 2010]. The typical long-term fault slip rate in subduction zones is of the order of 10^{-6} mm/s (a few centimeters per year), and the slip rate during SSEs is of the order of 10^{-5}–10^{-4} mm/s [e.g., *Dragert et al*., 2001; *Liu and Rice*, 2009; *Peng and Gomberg*, 2010]. We varied temperature from room temperature to 600°C. The deep limit of seismicity on subduction megathrusts is thought to occur at a temperature of about 350°C [*Hyndman and Wang*, 1993; *Gutscher and Peacock*, 2003], but estimates as low as 250°C and as high as 550°C have also been made [*Tichelaar and Ruff*, 1993]. For comparison, the deep limit of earthquake nucleation on continental transform faults is thought to occur at about 350°C [*Hyndman and Wang*, 1993; *Schwartz and Rokosky*, 2007; *Gutscher and Peacock*, 2003], and on oceanic transform faults at about 600°C based on seismic studies and thermal models [*McKenzie et al*., 2005; *Boettcher et al*., 2007]. For experiments in which the samples stably slid, we performed velocity steps between 3×10^{-4} and 3×10^{-2} mm/s, and directly measured the rate-state friction parameters $(a - b)$, a, D_c, and μ_o [*Dieterich*, 1978; *Ruina*, 1983]. For experiments in which the samples did not slide stably, we inverted for the respective parameters using the rate-state equations, as discussed in section 5.

3. Experimental Results

Figure 2 shows the evolution of shear stress of solid samples for the tested range of ambient temperatures (lowest temperatures tested are not shown since the samples slid stably). The data reveal a continuum of slip modes from stable sliding at low temperature (20–150°C), to oscillations and episodic slow slips in the mid temperature range (200–300°C), to robust unstable slip events at high temperature (350–600°C). Figure 3 shows the displacement histories of a few slip events so that the differences between slip events at different temperatures can be more easily distinguished. The slip velocity during experimental slow slip events is between 0.005 and 0.074 mm/s. This is between 5 and 70 times the load-point velocity. The geodetically inferred slip rates of SSEs (10^{-5} mm/s) exceed the long-term fault slip rates (10^{-6} mm/s) by the same order of magnitude, as noted in the previous section. SSE-like behavior in our laboratory experiments can be described by conditionally stable behavior of a one-dimensional spring-slider model with spring constant less than the critical stiffness. The slow slip events observed in our experiments, however, are not a direct analog to SSEs on natural faults, since slip on deformable faults involves a range of length scales (or stiffnesses) that control the degree of stability of sliding [e.g., *Rubin*, 2008].

We conducted additional tests on solid gabbro at 400°C and lower load-point velocities to explore if stick-slip behavior would still occur. The results of these experiments are shown in Figure 4. We find that the samples stick slipped and stress drops during slip events were larger for lower load-point velocities, even as low as 10^{-6} mm/s. This is presumably because the lower load-point velocity gives rise to more efficient healing between slip events, which allows for a greater stress drop during slip events, as expected by rate-state friction theory [*Dieterich*, 1978; *Ruina*, 1983; *Gu and Wong*, 1991; *He et al*., 2003]. For a given load-point velocity (10^{-3} mm/s), we also observe an increase in stress drop with temperature, similar to results of our tests on granite [*Mitchell et al*., 2013].

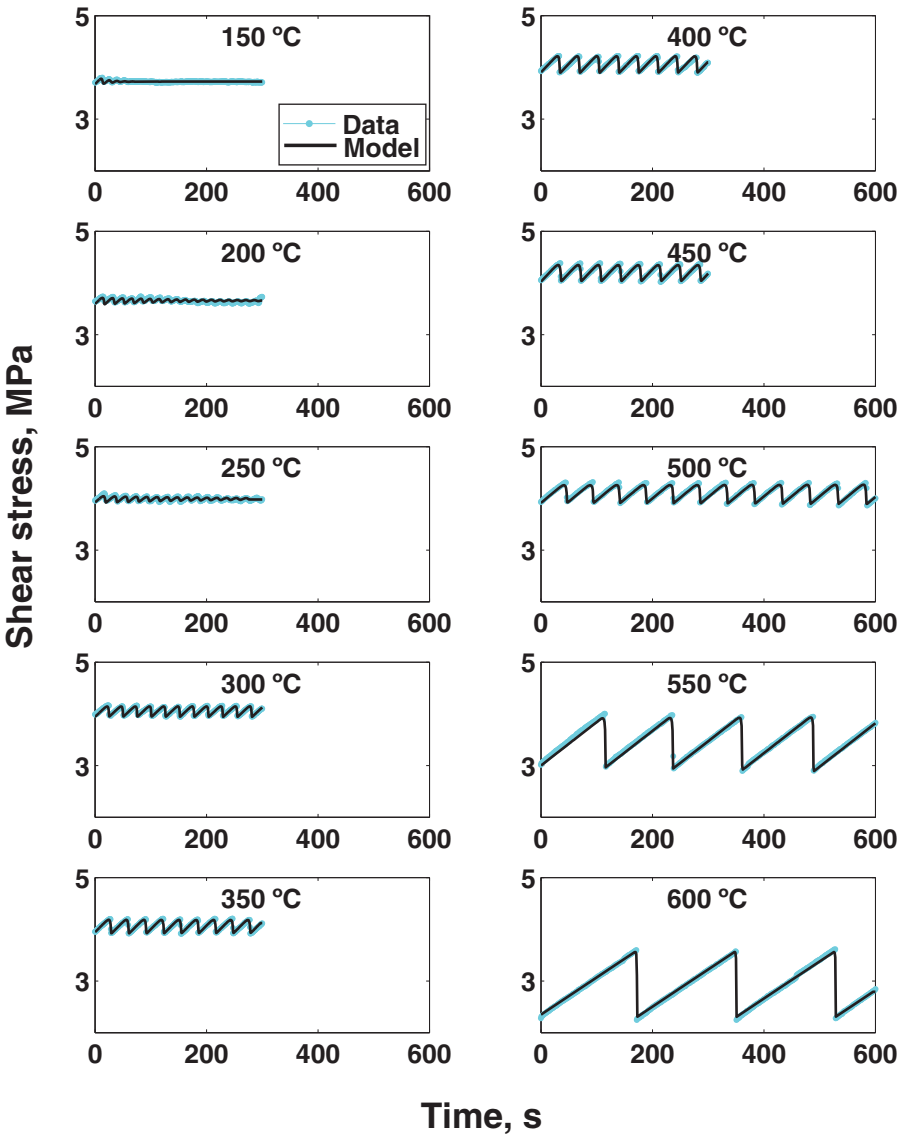

Figure 2. Shear stress time series. Cyan dotted lines represent shear stress data from experiments conducted on dry solid gabbro at normal stress of 5 MPa and load-point velocity of 10^{-3} mm/s. Black lines represent best fitting models.

We observed stable sliding in the dry simulated gouge samples at all temperatures. In the presence of water, at temperatures between 300 and 500°C, stable sliding transitioned to either episodic slow slips (in the case of 30 MPa normal stress) or stick-slip events (in the case of 5 MPa normal stress), as shown in Figure 5.

4. Shear Zone Microstructure

At the end of the experimental runs, we extracted both parts of the solid sample from the machine and glued them together with epoxy. We then sliced the sample perpendicular to the shear zone and created thin sections to investigate deformation microstructures within the shear zone. Figure 1c is a microscope image of a thin section that shows a portion of the shear zone, with shear direction indicated by the white arrow at the top of the figure. The shear surfaces look rough at the microscopic scale; between the shear surfaces is a layer of brown, very fine grained gouge material. The white arrows in Figure 1c point out possible Riedel shears within the gouge layer, indicating that deformation was occurring in the brittle regime. Figure 1d is a scanning electron microscope (SEM) image of the same thin section. Grain cracking can be seen along the edges of the shear zone, and gouge particles can be seen within the shear zone. The darker

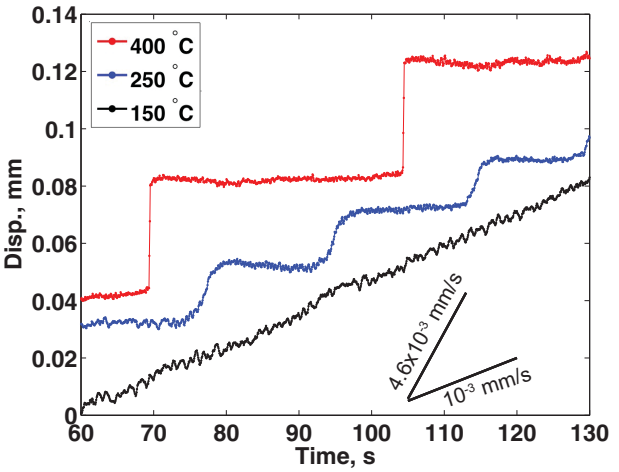

Figure 3. Displacement time series. Displacement data (offset added for visual clarity) as a function of time for experiments conducted on dry solid gabbro at three different temperatures. At 150°C, the sample slides stably at the driving speed of 10^{-3} mm/s. At 400°C, the sample exhibits stick-slip behavior, with maximum slip speed greater than 6.8 mm/s. At 250°C, the sample exhibits an intermediate SSE-like behavior, with slip speed of about 4.6×10^{-3} mm/s.

line running through the middle of the gouge zone is epoxy that intruded into the shear zone, possibly because strain was localized there during slip, causing the samples to separate along that plane when they were extracted from the machine. The inset image is a close up of the gouge material. It shows gouge particle size to be very small, of the order of about 100 nm.

5. Numerical Modeling

Due to the relatively low stiffness of the direct shear apparatus, we could not directly measure the rate-state friction parameters by performing velocity-stepping tests in case of unstable slip. Instead, we solved for the shear stress and displacement time series using a spring-slider model (Figure 1a) that incorporates the rate-state constitutive equations [*Dieterich*, 1978; *Ruina*, 1983]. We assume the following friction constitutive equation at the sliding interface,

$$\mu = \mu_o + a\ln\left(\frac{V}{V_o}\right) + b\ln\left(\frac{V_o\theta}{D_c}\right) \tag{1}$$

where μ is the coefficient of friction, V is the slip velocity, μ_o is the coefficient of friction at reference velocity V_o, a is the direct velocity effect, b is the evolution effect, θ is the state variable, and D_c is the slip weakening distance. This equation can be rewritten in terms of velocity as a function of coefficient of friction,

$$V = V_o\left(\frac{D_c}{V_o\theta}\right)^{\frac{b}{a}}\exp\left(\frac{\mu-\mu_o}{a}\right) \tag{2}$$

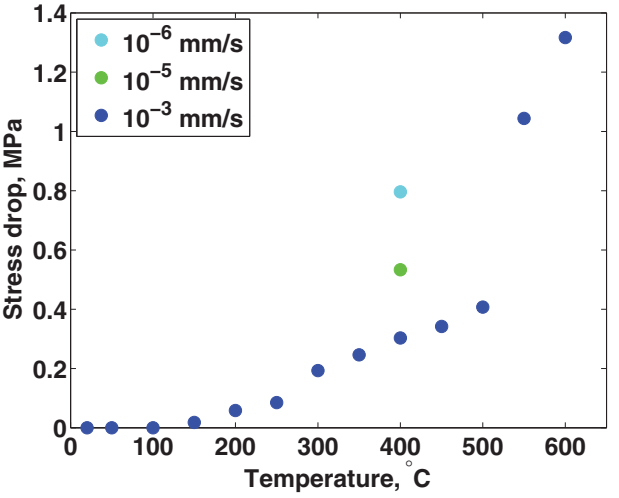

Figure 4. Stress drop. Stress drop during slip events as a function of temperature from an experiment conducted on dry solid gabbro at normal stress of 5 MPa. Dark blue dots represent data from experiments conducted at load-point velocity of 10^{-3} mm/s. We also conducted tests at 400°C and driving velocities of 10^{-5} and 10^{-6} mm/s, represented by green and cyan dots, respectively.

We have used several evolution laws for the state variable θ, including the aging law [*Dieterich*, 1978], the slip law [*Ruina*, 1983], a composite law [*Kato and Tullis*, 2001], and the aging law with a shear stress weakening term, c, as proposed by *Nagata et al.* [2012]:

$$\dot{\theta} = 1 - \frac{V\theta}{D_c}, \quad \text{Aging} \tag{3}$$

$$\dot{\theta} = -\frac{V\theta}{D_c}\ln\left(\frac{V\theta}{D_c}\right), \quad \text{Slip} \tag{4}$$

$$\dot{\theta} = \exp\left(\frac{-V}{V_c}\right) - \frac{V\theta}{D_c}\ln\left(\frac{V\theta}{D_c}\right), \quad \text{Composite} \tag{5}$$

$$\dot{\theta} = 1 - \frac{V\theta}{D_c} - \frac{c\theta}{\sigma b}\dot{\tau}, \quad \text{Modified aging} \tag{6}$$

In the composite law (equation (5)), V_c is a cutoff velocity, assumed to be 10^{-5} mm/s in our simulations. The rate of change in shear stress $\dot{\tau}$ is given by

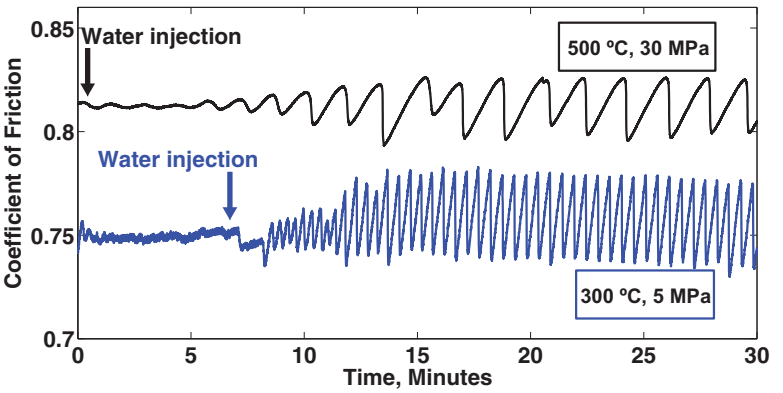

Figure 5. Dry and hydrated tests. (a) Coefficient of friction time series from tests conducted on simulated gabbro gouge. The black line represents a test conducted at 500°C and normal stress of 30 MPa. The blue line represents a test conducted at 300°C and normal stress of 5 MPa. Arrows represent the time at which water was injected into the bottom of the samples.

$$\dot{\tau} = k(V^* - V) \tag{7}$$

where k is the spring stiffness per unit contact area and V^* is the driving velocity. The different equations for evolution of the state variable were designed to empirically fit data from laboratory friction tests. The aging law (equation (3)), when applied to the spring-slider system, reproduces the increase in shear strength of the frictional interface with time. In this case, the state variable represents the average "lifetime" of asperities on the frictional interface [*Dieterich*, 1978; *Marone*, 1998]. In case of the slip law (equation (4)), both slip and slip velocity, not the time of contact time alone, affect coefficient of friction [*Ruina*, 1983; *Marone*, 1998]. The slip law fails to reproduce observed increases in static friction with time, but is able to explain a slip-weakening displacement that is independent of the magnitude and sign of abrupt velocity changes, as observed in laboratory tests [*Nakatani*, 2001; *Ampuero and Rubin*, 2008]. Both laws predict a steady state coefficient of friction at a constant velocity and a nearly instantaneous change in coefficient of friction due to a step-like change in velocity (in the same sign as the velocity change). The composite law (equation (5)) was proposed as a way to combine desirable aspects of the aging and slip laws. Below a cut-off velocity, V_c, it allows for time-dependent frictional healing, and above V_c it more closely approximates the slip law [*Kato and Tullis*, 2001]. The law proposed by *Nagata et al*. [2012] (equation (6)) includes a shear stress weakening term, c. *Nagata et al*. [2012] proposed that the values of a and b are actually much larger than traditionally estimated, and that a modification to the state variable evolution should be made to more appropriately fit the data.

The coupled system of equations (2) and (7) and the respective evolution law was solved using Matlab's stiff ordinary differential equation solver "ode23s" subject to initial conditions of $[\delta_o, \tau_o, \theta_o] = [0, \mu_o\sigma, D_c/V_o]$, where δ is slip. The predicted shear stress time series was shifted in time to achieve the best agreement (using cross correlation) with the observed shear stress time series. The shift is necessary because the observed time series begins at an arbitrary point during the stick-slip cycle. The misfit between the two time series was then evaluated by computing the sum of the squares of the difference between the data and the model. This process was repeated for a range of values of the rate-state parameters $(a-b)$, $(a+b)$, D_c, and μ_o (and c in case of the modified aging law). The best fitting parameter values were chosen to be those that rendered the smallest misfit. This process was repeated for data from experiments conducted at different temperatures.

All of the models are able to fit the data at low temperatures, when friction is nearly velocity neutral. Differences in the models become significant at higher temperatures, when sliding becomes increasingly unstable (Figure 6). At high temperatures, the best fit is obtained using the aging law. It reproduces the relatively constant displacement during "stick" intervals, as well as large stress drops during slip events. This model does a good job of reproducing the abruptness of slip events, although at the highest temperatures it still underpredicts the velocity during slip events. The model incorporating the slip law, on the other hand, overpredicts creep during "stick" intervals and underpredicts stress drops during slip events. The slip events predicted by this model are much less abrupt than those predicted

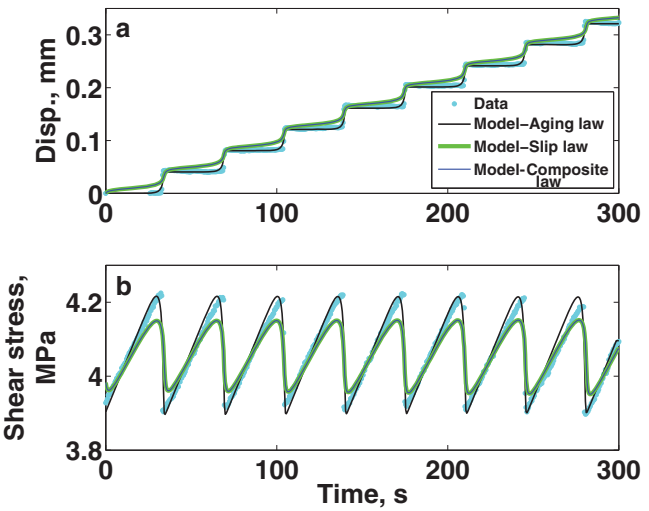

Figure 6. Evolution Laws. (a) Displacement time series. (b) Shear stress time series. Cyan dots represent data from a test on solid gabbro at normal stress of 5 MPa, temperature of 400°C, and load-point velocity of 10^{-3}. Black lines represents best fitting model incorporating the aging law. Green lines represent best fitting model incorporating the slip law. Dark blue lines (coincident with green lines) represent best fitting model incorporating the composite law.

by the model incorporating the aging law. The model incorporating the composite law produces results very similar to those of the slip law. The model incorporating the stress-weakening parameter, c, produces the smallest misfit to the data when $c = 0$, which is the same as the aging law. Models that best fit the data from solid gabbro samples (assuming the aging law) are shown as black lines in Figure 2.

6. Results: Rate-State Parameters

6.1. Dry Solid Gabbro

Figure 7 shows the best estimates for the rate parameter $(a - b)$ as a function of temperature. Figure 8 shows our best estimates for the parameters a, b, μ_{ss} (at $V = 10^{-2}$ mm/s), and D_c. These values are summarized in Table 1. At 150°C, the solid gabbro data show a transitional (near velocity-neutral) behavior with small oscillations in shear stress that decay with time to stable sliding. This allows us to use both methods (velocity stepping and parameter fitting) to determine the rate-state parameters of interest. We find that the results of the two methods are in agreement within the uncertainties (Figure 7). For solid gabbro samples, we observe a decrease in $(a - b)$ with temperature, from 0.002 at 20°C to −0.040 at 600°C, with a transition from velocity strengthening to velocity weakening around 150°C. A decreasing trend in $(a - b)$ is necessary to fit the more unstable sliding behavior at higher temperature, which is characterized by longer recurrence intervals, larger stress drops, and faster slip events. We find that a is nearly independent of temperature between 20 and 500°C and equal to about 0.004, and decreases with temperature between 500 and 600°C to about 0.0009. Parameter b increases with temperature from 0.004 at 20°C to 0.020 at 500°C and sharply increases to 0.041 at 600°C. Our inversions suggest a small increase in D_c with temperature from 7 μm at 20°C to 8 μm at 500°C, and a large increase to 33 μm at 600°C. The increase in D_c is needed to fit the larger recurrence interval between slip events at higher temperature. We observe a small increase in μ_o with temperature from 0.75 at 20°C to 0.78 at 500°C, and a decrease to 0.55 at 600°C.

6.2. Simulated Gabbro Gouge at Dry and Hydrated Conditions

For dry simulated gouge samples, we observe a comparatively small decrease in $(a - b)$ from 0.0015 at 20°C to −0.0031 at 600°C, with a transition to velocity weakening at about 150°C. We do not observe a significant difference in $(a - b)$ for data collected at normal stress of 5 versus 30 MPa. We find that a is relatively constant at ∼0.005 between 20 and 400°C, and increases to 0.007 at 600°C. b increases from 0.005 at 20°C to 0.012 at 600°C. Both a and b are slightly larger for tests conducted at normal stress of 5 MPa compared to tests conducted at 30 MPa. We do not observe a consistent trend in μ_{ss} with temperature. While the uncertainty in our measurements for D_c is very high, there does seem to be a small increase in D_c with temperature from 500 to 600°C. D_c is consistently higher for tests conducted at 30 MPa ($D_c \sim 0.05$ mm) versus 5 MPa ($D_c \sim 0.02$ mm). Overall, estimates for D_c from granular samples are higher than those from solid samples. For hydrated gouge samples, $(a - b)$ is slightly lower than for dry gouge samples. The more negative values of $(a - b)$ in hydrated tests are obvious from unstable sliding (compared to stable sliding in dry tests). a and b are individually both higher for hydrated tests compared to dry tests. There is no consistent trend in μ_{ss} with temperature in hydrated gouge tests. Estimates of D_c are lower for tests conducted on hydrated versus dry gouge.

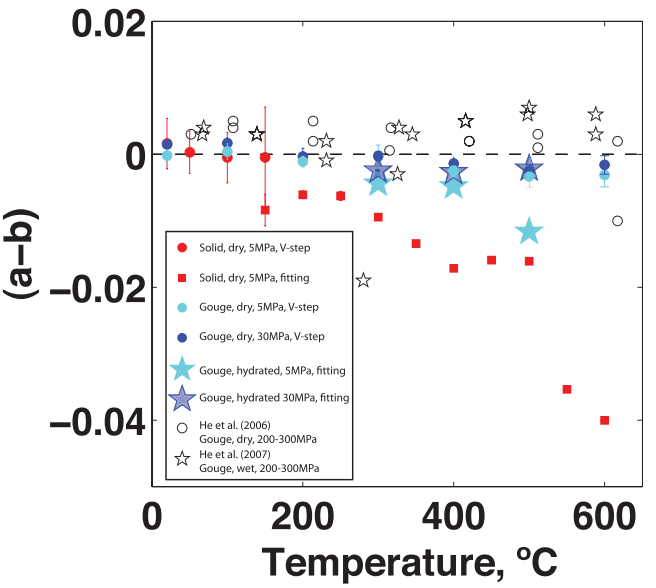

Figure 7. $(a - b)$ versus temperature. Open symbols denote results from previous studies. Filled symbols denote results from this study. Error bars on symbols representing velocity-stepping tests correspond to two standard deviations. Error bars on symbols representing model fits to the time series correspond to the variation in $(a - b)$ that triples the minimum misfit at a given temperature.

7. Discussion

7.1. Micromechanical Context of the Rate, State, and Temperature Dependence of Frictional Properties

Some features of the temperature dependence of friction parameters can be explained in terms of adhesion theory [*King and Marone*, 2012; *Mitchell et al.*, 2013]. According to adhesion theory, the macroscopic friction coefficient is controlled by the area and the shear strength of microscopic contact asperities [*Bowden and Tabor*, 1950; *Dieterich and Kilgore*, 1994]. Contact area may increase at higher temperatures due to enhanced creep and flattening of asperities [*Mitchell et al.*, 2013]. This can explain the inferred increase in D_c, the characteristic asperity size, with temperature. Greater values of D_c for tests conducted on simulated gouge at 30 versus 5 MPa might be due to greater flattening of asperities under higher normal stress, or more efficient packing of gouge particles. If so, the inferred lower values of D_c of hydrated gouge compared to those of dry gouge are surprising, since increased water content is expected to decrease viscosity, and increase the creep rate. One possibility is that values of D_c inferred from numerical modeling are systematically underestimated compared to values of D_c directly estimated from velocity-stepping tests. Note that values of D_c estimated using velocity-stepping tests are similar at comparable temperatures for solid samples under dry conditions and gouge samples under hydrated conditions (Figure 7d). There is a certain trade-off between $(a - b)$ and D_c in models of unsteady slip. This trade-off is related to a condition for instability that defines a critical stiffness below which oscillations begin to grow. The critical stiffness, k_{crit}, depends on the ratio of $(a - b)$ and D_c ($k_{crit} = \sigma_n \frac{-(a-b)}{D_c}$) [*Ruina*, 1983]; these parameters are highly covariant in numerical models of oscillatory slip (Figure 9).

We do not observe a consistent trend in coefficient of friction, μ_{ss}, with temperature (Figure 7c). This may be explained by a trade-off between decreases in shear strength of asperities [*Blanpied*, 1995] and increases in the asperity size, as the coefficient of friction depends on both the asperity contact area and asperity strength.

It has been argued based on adhesion theory that the so-called "aging effect" (a logarithmic increase in shear strength withhold time) is due to the flattening of asperities in time under a given normal load [*Bowden and Tabor*, 1950; *Dieterich*, 1972; *Dieterich and Kilgore*, 1994]. The rate of the "aging effect" is controlled by the evolution parameter b. At higher temperatures, asperities may deform more quickly, leading to a faster increase in contact area under normal load. This could be a primary control on the inferred increase in b with temperature [*Mitchell et al.*, 2013]. We do not observe a consistent trend in a with temperature, despite the theoretical prediction that a should linearly increase with temperature [*Heslot et al.*, 1994; *Sleep*, 1997; *Nakatani*, 2001].

7.2. Comparison With Previous Experimental Results

The downdip limit of the seismogenic zone on subduction megathrusts (depth of ~30–70 km, temperature of ~350–600°C) is thought to be controlled by a transition to velocity-strengthening friction [e.g., *Liu and Rice*, 2009]. Available experimental data indicate that gabbro transitions from velocity weakening to velocity strengthening at a temperature of 310 and 510°C for nonsupercritical and supercritical water conditions, respectively, under effective normal stress of 130–200 MPa. This is close to the estimated temperatures at the deep limit of the seismicity on subduction megathrusts, in the source region of SSEs. However, at higher

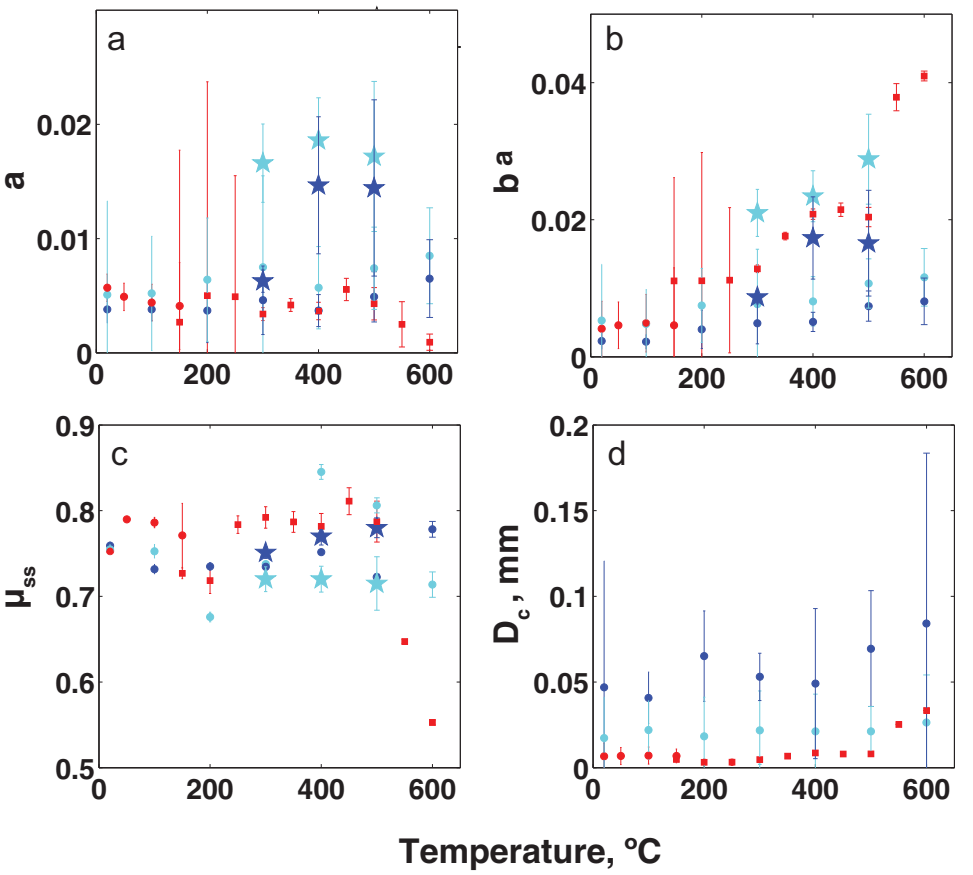

Figure 8. Rate-state parameters versus temperature. Symbols are the same as those in Figure 7. (a) *a*. (b) *b*. (c) μ_{ss} at V = 10^{-2} mm/s. (d) D_c.

normal stress (300 MPa), velocity strengthening was observed at all temperatures. This is in contrast to our results that show progressive velocity weakening with temperature up to 600°C. One possible reason for the discrepancy between our results and those of *He et al*. [2007] might be related to subtle differences in sample mineralogy. The gabbro samples of *He et al*. [2007] contained a small fraction of quartz, while we did not identify quartz in our gabbro samples. A more recent study demonstrated that gouges composed of plagioclase and pyroxene (the dominant minerals in gabbro) were velocity weakening at temperatures up to 600°C, but the addition of a small amount (3–5%) of quartz caused velocity-strengthening friction between 400 and 600°C [*He et al*., 2013]. We do not believe that compositional variations alone are a viable explanation, as our experiments on Westerly granite, which has a significant fraction of quartz, revealed velocity weakening and unstable slip at high temperature [*Mitchell et al*., 2013; E. Mitchell et al., What controls the depth distribution of earthquakes in the Earth's crust?, submitted manuscript, Nature, 2015]. Another reason for the discrepancy between our results and those of *He et al*. [2007] may be related to differences in the experimental apparatuses. The experiments of *He et al*. [2007] were conducted using a triaxial apparatus, which can produce large normal stress and high pore pressure, but is limited to only a few millimeters of total displacement on the samples. The direct shear apparatus can achieve larger total displacements (order of 10–10^2 mm in individual runs), but smaller normal stresses (up to 40 MPa) and pore pressures (not exceeding the atmospheric pressure because the samples are unconfined). In the study of *He et al*. [2006], velocity-strengthening behavior was observed in dry gabbro at all temperatures, and ($a - b$) was reported to be in the range of 0.001–0.005, except for one test that exhibited unstable slip and large negative ($a - b$) at 610°C. One possibility is that a limited total displacement in triaxial tests might have biased the results toward velocity-strengthening behavior. It is well known that the development of a fabric within the gouge layer due to slip localization encourages the transition to velocity weakening with

Table 1. Rate-State Parameters[a]

Sample Type	Water	σ_n (MPa)	Method	T (°C)	$(a-b)$	a	b	μ_{ss}	D_c (mm)
Solid	Dry	5	v-step	20	0.0016	0.0057	0.0041	0.753	0.0066
Solid	Dry	5	v-step	50	0.0003	0.0049	0.0046	0.790	0.0068
Solid	Dry	5	v-step	100	−0.0005	0.0044	0.0049	0.786	0.0071
Solid	Dry	5	v-step	150	−0.0005	0.0041	0.0046	0.771	0.0069
Solid	Dry	5	Fit	150	−0.0084	0.0027	0.0111	0.727	0.0048
Solid	Dry	5	Fit	200	−0.0061	0.005	0.0111	0.718	0.0031
Solid	Dry	5	Fit	250	−0.0063	0.0049	0.0112	0.784	0.0032
Solid	Dry	5	Fit	300	−0.0095	0.0034	0.0129	0.792	0.0047
Solid	Dry	5	Fit	350	−0.0134	0.0042	0.0176	0.787	0.0067
Solid	Dry	5	Fit	400	−0.0172	0.0037	0.0209	0.782	0.0086
Solid	Dry	5	Fit	450	−0.0159	0.0055	0.0214	0.811	0.0080
Solid	Dry	5	Fit	500	−0.0161	0.0043	0.0204	0.787	0.0080
Solid	Dry	5	Fit	550	−0.0354	0.0025	0.0379	0.647	0.0252
Solid	Dry	5	Fit	600	−0.04	0.0009	0.0409	0.5530	0.0334
Gouge	Dry	5	v-step	20	−0.0002	0.0051	0.0053	0.755	0.0173
Gouge	Dry	5	v-step	100	0.0004	0.0052	0.0048	0.753	0.0220
Gouge	Dry	5	v-step	200	−0.0011	0.0064	0.0075	0.676	0.0183
Gouge	Dry	5	v-step	300	−0.0002	0.0075	0.0077	0.738	0.0218
Gouge	Dry	5	v-step	400	−0.0024	0.0057	0.0081	0.845	0.0211
Gouge	Dry	5	v-step	500	−0.0033	0.0074	0.0107	0.806	0.0213
Gouge	Dry	5	v-step	600	−0.0031	0.0085	0.0116	0.714	0.0263
Gouge	Dry	30	v-step	20	0.0015	0.0038	0.0023	0.759	0.0469
Gouge	Dry	30	v-step	100	0.0017	0.0038	0.0021	0.732	0.0408
Gouge	Dry	30	v-step	200	−0.0003	0.0037	0.0040	0.735	0.0651
Gouge	Dry	30	v-step	300	−0.0003	0.0046	0.0049	0.734	0.0530
Gouge	Dry	30	v-step	400	−0.0014	0.0037	0.0051	0.752	0.0491
Gouge	Dry	30	v-step	500	−0.0025	0.0049	0.0074	0.723	0.0695
Gouge	Dry	30	v-step	600	−0.0016	0.0065	0.0081	0.778	0.0842
Gouge	Hydrated	5	Fit	300	−0.0044	0.0166	0.0210	0.720	0.0020
Gouge	Hydrated	5	Fit	400	−0.0048	0.0186	0.0234	0.720	0.0022
Gouge	Hydrated	5	Fit	500	−0.0116	0.0172	0.0288	0.715	0.0049
Gouge	Hydrated	30	Fit	300	−0.0024	0.0063	0.0087	0.751	0.0056
Gouge	Hydrated	30	Fit	400	−0.0027	0.0147	0.0174	0.770	0.0051
Gouge	Hydrated	30	Fit	500	−0.0021	0.0144	0.0165	0.780	0.0048

[a]Direct measurements from velocity-stepping tests or best fitting rate-state friction parameters, as plotted in Figures 7 and 8.

increasing slip [*Gu and Wong*, 1994; *Beeler et al.*, 1996]. For example, *Marone and Cox* [1994] reported velocity-strengthening behavior ($(a-b)=0.005$) that transitioned to velocity-weakening behavior ($(a-b)=-0.001$) as total displacement increased to more than 50 mm in their tests conducted on gabbro at room temperature with a large direct-shear apparatus. Studies on granite gouge also show decreases in $(a-b)$ in the first few millimeters of total slip [*Dieterich*, 1981; *Biegel et al.*, 1989; *Collettini et al.*, 2009]. Our experiments on solid gabbro at room temperature show a similar behavior, although we observed that heating and subsequent cooling may increase $(a-b)$, presumably due to a reduction in water content. The absence of well-developed shear fabric in triaxial experiments on gabbro at high temperatures [*Stesky et al.*, 1974; *He et al.*, 2006] could bias the results toward greater velocity strengthening compared to our experiments. To test this possibility, we performed additional experiments on solid samples of gabbro in which we removed the wear products from the slip interface and reroughened the surface with 80 grit paper. These experiments still exhibited stick-slip behavior at high temperature and low (<10 mm) displacement. Hence, the difference in the inferred values of $(a-b)$ in our experiments and triaxial experiments at high temperature cannot be completely attributed to shear fabric development. Another possibility is that the inferred frictional properties are affected by the experimental design. For example, in the direct-shear setup, a small amount of torque on the moving (top) sample holder might give rise to nonuniform distribution of normal stress along the shear zone. In triaxial experiments, the results could be affected by the interaction of the confining jacket with the sample. Velocity dependence of friction may be also affected by pore pressure. Triaxial experiments conducted on gabbro and granite at both dry and hydrothermal conditions indicate that the addition of water enhances velocity weakening at temperatures between 150 and 350°C and velocity strengthening at temperatures above ~350–450°C [*Blanpied et al.*, 1991; *He et al.*, 2006, 2007]. In our experiments, the addition of water enhances velocity weakening at temperatures up to 500°C. This discrepancy might be attributed to water fugacity. In particular, high water fugacity is expected to enhance

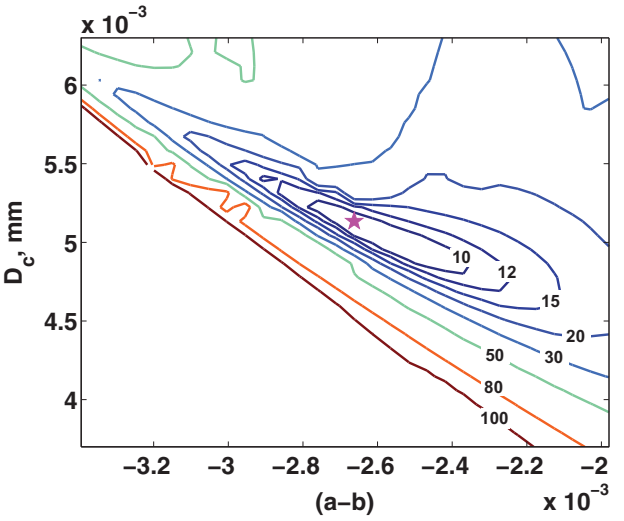

Figure 9. Trade-off between ($a - b$) and D_c. Misfit between shear stress time series and numerical predictions as a function of the rate-state parameters ($a - b$) and D_c. Shear stress data are from an experiment conducted on hydrated gabbro gouge at temperature of 400°C, normal stress of 30 MPa and load-point velocity of 10^{-3} mm/s.

hydrolytic reactions that might give rise to stable creep [*Keefner et al*., 2011; *Mei and Kohlstedt*, 2000a,b]. This, however, cannot explain the discrepancy in ($a - b$) between the direct shear and triaxial experiments conducted at dry conditions (Figure 7). Further insights into possible causes of a disagreement between results obtained on different apparatus may be gained, for example, by conducting triaxial experiments over a wider range of normal stresses, including low-to-intermediate (1–100 MPa) normal stresses, and variable water fugacities over a range of elevated temperatures.

7.3. Implications for Natural SSEs in Subduction Zones

Results from our experiments suggest that the temperature dependence of frictional properties of gabbro alone may not explain the occurrence of slow slip events at the base of the seismogenic zone in subduction settings. It is likely that a number of factors such as temperature, water content, water fugacity, mineral composition, shear fabric, gouge thickness, and lithologic heterogeneity all affect the value of ($a - b$) and the degree of locking and stability of the fault interface. Among previously suggested mechanisms for slow slip events in subduction zones is the dependence of ($a - b$) on slip velocity. For example, if ($a - b$) is negative at low slip velocity but positive at a higher (but still subseismic) velocity, a slip event could nucleate but not accelerate to become an earthquake. *Kaproth and Marone* [2013] reported such behavior in double direct shear experiments conducted at room temperature on serpentinite. In their experiments, the transition from negative to positive ($a - b$) occurred at slip rate of $\sim 10^{-2}$ mm/s. We did not observe a dependence of ($a - b$) on sliding velocity in our velocity-stepping tests on gabbro over the tested range of velocities up to 3×10^{-2} mm/s. We cannot rule out a possibility that ($a - b$) could change sign at velocities that are greater still.

In fact, it is not clear if gabbro is a representative rock type of the slip interface on subduction megathrusts [*Plank and Langmuir*, 1998]. It has been suggested that compositions rich in clays and phyllosilicates such as smectite (from the accretionary prism), illite (the low-grade metamorphic product of smectite), chlorite, and muscovite may be present on the megathrust interface and affect the slip behavior of the fault [*Ikari et al*., 2009; *Carpenter et al*., 2011; *Schleicher et al*., 2012]. This may pose a problem for explaining seismogenic behavior, since clays are known to be velocity strengthening [*Saffer and Marone*, 2003; *Ikari et al*., 2009], although a possibility of a transition to velocity weakening was suggested due to processes such as consolidation and cementation [*Moore and Saffer*, 2001; *Saffer and Marone*, 2003]. While velocity-strengthening regions of the fault cannot nucleate ruptures, it is possible that ruptures could nucleate in a nearby velocity-weakening region and propagate into velocity-strengthening (clay rich) regions due to stress perturbations [*Perfettini and Ampuero*, 2008; *Kaneko et al*., 2008; *Faulkner et al*., 2011]. There is geological evidence that the long-term motion on a megathrust deforms accretionary prism sediments as well as the top of the oceanic basement. Blocks of basalt intermixed with sediments have been documented in melanges in the Shimanto Belt in western Japan [*Kimura and Mukai*, 1991]. Some of these melanges may have formed at temperatures corresponding to the deep limit of the seismogenic zone (350°C), since they are thought to have been underplated under greenschist metamorphic conditions [*Kimura and Mukai*, 1991]. Other melanges in the Shimanto Belt contain unaltered basalts [*Kimura and Mukai*, 1991]. This could either be an indication of melange formation at shallower depths, or an indication that water fugacity was low during formation, since olivine serpentinization would have occurred under hydrothermal conditions [*Malvoisin et al*., 2012].

A mixture of velocity-weakening and velocity-strengthening lithologies could potentially produce SSEs [*Den Hartog et al*., 2012; *Saffer and Wallace*, 2015]. In particular, *Den Hartog et al*. [2012] showed that a certain

mixture of illite and quartz can produce a transition from velocity weakening to velocity strengthening at temperatures that correspond to a transition between locked and creeping parts of subduction megathrusts. Microstructural analysis of the gouge mixture deformed at high temperatures revealed significant deformation within illite, and no evidence of quartz plasticity, suggesting that phyllosilicates may play an important role in the stability transition at the bottom of the seismogenic zone [*Den Hartog et al.*, 2012]. Clay-rich lithologies are known to influence the degree of fault locking on continental transform faults. For instance, core samples from the San Andreas Fault Observatory at Depth (SAFOD) revealed foliated chlorite-smectite and illite assemblages that that may control fault creep down to depth of 10 km [*Schleicher et al.*, 2012]. In subduction settings, clays and phyllosilicates may be introduced on the megathrust interface from the downgoing oceanic sediments. Alternatively, they can be derived from the oceanic crust during a transformation of gabbro to greenschist facies. This transformation is expected to occur at temperatures of ~300–450°C and pressures of ~200–1000 MPa, which are coincident with temperatures and pressures in the source region of slow slip events at the downdip end of shallow seismicity in subduction zones.

7.4. Implications for Faulting in Other Tectonic Settings

The frictional properties of gabbro measured in this study are also relevant to our understanding of mechanics of oceanic transform faults. One feature of interest is the degree of seismic coupling on oceanic transform faults. For instance, as much as 85% of slip above the 600°C isotherm in the oceanic lithosphere is thought to occur aseismically based on comparisons of seismic moment release rate and moment accumulation due to relative plate motion [*Boettcher and Jordan*, 2004]. Our results for gabbro gouge indicate velocity-strengthening behavior below 200°C, and weakly velocity-weakening behavior between 400 and 600°C (Figure 7), which may help explain the low seismic coupling throughout the entire oceanic crust [*Boettcher and Jordan*, 2004]. At greater depths, a transition to velocity strengthening in olivine above 600°C is thought to explain the deep limit of the seismogenic zone in the mantle [*Boettcher et al.*, 2007]. This interpretation implies robust creep in the top several kilometers of oceanic transforms following large earthquakes and in the interseismic period. Another relevant observation is an increase in the characteristic slip-weakening distance, D_c, with temperature and normal stress (Figure 8d). An increase in D_c with depth was postulated in numerical models of earthquake cycles on oceanic transform faults in order to reproduce the low seismic coupling observed on both short, high slip rate and long, low slip rate oceanic transform faults [*Liu et al.*, 2012]. Our experimental results (Figure 8d) lend support to the hypothesis that increases in D_c with depth can play an important role in the partitioning of aseismic and seismic slip on oceanic transform faults.

On continents, seismicity is generally limited to the silicic upper crust, while the mafic lower crust is dominantly aseismic [*Eaton et al.*, 1970; *Hill et al.*, 1975; *Wesson et al.*, 1973; *Sibson*, 1982; *Tse and Rice*, 1986; *Blanpied et al.*, 1991]. However, deep lower crustal seismicity has been reported in regions of active extension [*Craig et al.*, 2011; *Emmerson et al.*, 2006] and convergence [*Jackson*, 2002; *Leyton et al.*, 2009]. Our results indeed indicate that the lower continental crust can allow nucleation of slip instabilities under dry or low water fugacity conditions (Figure 7). As slip rate increases, a number of dynamic weakening mechanisms can promote seismic ruptures, as observed in laboratory experiments [*Hirose and Shimamoto*, 2005; *Di Toro et al.*, 2011; *Niemeijer et al.*, 2011; *Brown and Fialko*, 2012] and in nature [*Di Toro et al.*, 2006].

8. Conclusions

We conducted a series of friction experiments on gabbro at conditions thought to be representative of slow slip events at subduction zones. For dry solid samples of gabbro, we observed stable sliding at low temperatures (20–150°C), episodic slow slips in the mid temperature range (200–300°C), and stick slip at high temperatures (350–600°C). For dry gouge samples, we observed stable sliding at all temperatures. For hydrated gouge samples, we observed episodic slow slip and stick slip at high temperatures (300–500°C). For experiments in which the samples stably slid, we conducted velocity-stepping tests and directly measured the rate-state parameters. For experiments in which the samples exhibited time-dependent sliding, we performed a grid search for the parameter values that provided the best numerical fit to the recorded shear stress time series. We find that $(a - b)$ is small and positive (~0.001) at room temperature for solid and gouge samples. Parameter $(a - b)$ decreases with temperature to −0.040 at 600°C for dry solid samples and to −0.003 for dry gouge samples. $(a - b)$ is more negative for hydrated gouge samples compared to

dry gouge samples. We do not observe a high-temperature transition to velocity strengthening, which is thought to control the deep limit of seismogenic zones and the extent of SSEs. Other factors such as the presence of clay-rich sediments, transformation of gabbro to greenschist facies (which include velocity-strengthening clay minerals such as chlorite, smectite, illite, and muscovite) may govern the occurrence of slow slip events at the base of the seismogenic zone on subduction megathrusts.

Notation

μ Coefficient of friction, dimensionless.
μ_o Reference coefficient of friction, dimensionless.
V_o Reference velocity or slip rate, mm/s.
μ_{ss} Steady state coefficient of friction, dimensionless.
V Velocity or slip rate, mm/s.
a Direct velocity effect, dimensionless.
b Evolution effect, dimensionless.
θ State variable, s.
D_c Slip weakening distance, mm.
V_c Cutoff velocity or slip rate, mm/s.
τ Shear stress, MPa.
$\dot{\tau}$ Rate of change of shear stress, MPa/s.
k Machine stiffness, MPa/mm.
V^* Driving velocity, mm/s.
σ Normal stress, MPa.
c Shear stress weakening parameter, dimensionless.

Acknowledgments
This work was supported by NSF (grants EAR-0838255 and 1321932). The best estimates for the rate-state parameters and some of the laboratory recorded time series can be found in the figures and table in this manuscript. The rest of the laboratory time series can be downloaded from igppweb.ucsd.edu/~fialko/data.html, or via email at ekmitche@ucsd.edu. Thanks to the two reviewers who provided useful comments and thoughtful suggestions on an earlier version of the manuscript.

References

Ampuero, J.-P., and A. M. Rubin (2008), Earthquake nucleation on rate and state faults–Aging and slip laws, *J. Geophys. Res.*, *113*, B01302, doi:10.1029/2007JB005082.
Bartlow, N. M., S. Miyazaki, A. M. Bradley, and P. Segall (2011), Space-time correlation of slip and tremor during the 2009 Cascadia slow slip event, *Geophys. Res. Lett.*, *38*, L18309, doi:10.1029/2011GL048714.
Beeler, N., T. Tullis, M. Blanpied, and J. Weeks (1996), Frictional behavior of large displacement experimental faults, *J. Geophys. Res.*, *101*(B4), 8697–8715.
Biegel, R. L., C. G. Sammis, and J. H. Dieterich (1989), The frictional properties of a simulated gouge having a fractal particle distribution, *J. Struct. Geol.*, *11*(7), 827–846.
Blanpied, M., D. Lockner, and J. Byerlee (1991), Fault stability inferred from granite sliding experiments at hydrothermal conditions, *Geophys. Res. Lett.*, *18*(4), 609–612.
Blanpied, M. L. (1995), Frictional slip of granite at hydrothermal conditions, *J. Geophys. Res.*, *100*(B7), 13,045–13,064.
Boettcher, M. S., and T. Jordan (2004), Earthquake scaling relations for mid-ocean ridge transform faults, *J. Geophys. Res.*, *109*, B12302, doi: 10.1029/2004JB003110.
Boettcher, M. S., G. Hirth, and B. Evans (2007), Olivine friction at the base of oceanic seismogenic zones, *J. Geophys. Res.*, *112*, B01205, doi: 10.1029/2006JB004301.
Bowden, F. P., and D. Tabor (1950), *The Friction and Lubrication of Solids*, Clarendon, Oxford, U. K.
Brown, K. M., and Y. Fialko (2012), Melt welt mechanism of extreme weakening of gabbro at seismic slip rates, *Nature*, *488*(7413), 638–641.
Carpenter, B., C. Marone, and D. Saffer (2011), Weakness of the San Andreas Fault revealed by samples from the active fault zone, *Nat. Geosci.*, *4*(4), 251–254.
Cervelli, P., P. Segall, K. Johnson, M. Lisowski, and A. Miklius (2002), Sudden aseismic fault slip on the south flank of Kilauea volcano, *Nature*, *415*(6875), 1014–1018.
Collettini, C., A. Niemeijer, C. Viti, and C. Marone (2009), Fault zone fabric and fault weakness, *Nature*, *462*(7275), 907–910.
Craig, T., J. Jackson, K. Priestley, and D. McKenzie (2011), Earthquake distribution patterns in Africa: Their relationship to variations in lithospheric and geological structure, and their rheological implications, *Geophys. J. Int.*, *185*(1), 403–434.
Den Hartog, S., A. Niemeijer, and C. Spiers (2012), New constraints on megathrust slip stability under subduction zone P–T conditions, *Earth Planet. Sci. Lett.*, *353*, 240–252.
Dieterich, J. H. (1972), Time-dependent friction in rocks, *J. Geophys. Res.*, *77*(20), 3690–3697.
Dieterich, J. H. (1978), Time-dependent friction and the mechanics of stick-slip, *Pure Appl. Geophys.*, *116*(4-5), 790–806.
Dieterich, J. H. (1981), Constitutive properties of faults with simulated gouge, in *Mechanical Behavior of Crustal Rocks: The Handin Volume*, AGU, Washington, D. C., pp. 103–120.
Dieterich, J. H., and B. D. Kilgore (1994), Direct observation of frictional contacts: New insights for state-dependent properties, *Pure Appl. Geophys.*, *143*(1-3), 283–302.
Di Toro, G., T. Hirose, S. Nielsen, G. Pennacchioni, and T. Shimamoto (2006), Natural and experimental evidence of melt lubrication of faults during earthquakes, *Science*, *311*(5761), 647–649.

Di Toro, G., R. Han, T. Hirose, N. De Paola, S. Nielsen, K. Mizoguchi, F. Ferri, M. Cocco, and T. Shimamoto (2011), Fault lubrication during earthquakes, *Nature*, *471*(7339), 494–498.
Dobson, D. P., P. G. Meredith, and S. A. Boon (2002), Simulation of subduction zone seismicity by dehydration of serpentine, *Science*, *298*(5597), 1407–1410.
Dragert, H., K. Wang, and T. S. James (2001), A silent slip event on the deeper Cascadia subduction interface, *Science*, *292*(5521), 1525–1528.
Eaton, J., M. O'neill, and J. Murdock (1970), Aftershocks of the 1966 Parkfield-Cholame, California, earthquake: A detailed study, *Bull. Seismol. Soc. Am.*, *60*(4), 1151–1197.
Emmerson, B., J. Jackson, D. McKenzie, and K. Priestley (2006), Seismicity, structure and rheology of the lithosphere in the Lake Baikal region, *Geophys. J. Int.*, *167*(3), 1233–1272.
Faulkner, D., T. Mitchell, J. Behnsen, T. Hirose, and T. Shimamoto (2011), Stuck in the mud? Earthquake nucleation and propagation through accretionary forearcs, *Geophys. Res. Lett.*, *38*, L18303, doi:10.1029/2011GL048552.
Gu, Y., and T.-F. Wong (1991), Effects of loading velocity, stiffness, and inertia on the dynamics of a single degree of freedom spring-slider system, *J. Geophys. Res.*, *96*(B13), 21,677–21,691.
Gu, Y., and T.-F. Wong (1994), Development of shear localization in simulated quartz gouge: Effect of cumulative slip and gouge particle size, *Pure Appl. Geophys.*, *143*(1-3), 387–423.
Gutscher, M.-A., and S. M. Peacock (2003), Thermal models of flat subduction and the rupture zone of great subduction earthquakes, *J. Geophys. Res.*, *108*(B1), 2009, doi:10.1029/2001JB000787.
Hacker, B. R., S. M. Peacock, G. A. Abers, and S. D. Holloway (2003), Subduction factory: 2. Are intermediate-depth earthquakes in subducting slabs linked to metamorphic dehydration reactions?, *J. Geophys. Res.*, *108*(B1), 2030, doi:10.1029/2001JB001129.
He, C., T.-F. Wong, and N. M. Beeler (2003), Scaling of stress drop with recurrence interval and loading velocity for laboratory-derived fault strength relations, *J. Geophys. Res.*, *108*(B1), 2037, doi:10.1029/2002JB001890.
He, C., W. Yao, Z. Wang, and Y. Zhou (2006), Strength and stability of frictional sliding of gabbro gouge at elevated temperatures, *Tectonophysics*, *427*(1), 217–229.
He, C., Z. Wang, and W. Yao (2007), Frictional sliding of gabbro gouge under hydrothermal conditions, *Tectonophysics*, *445*(3), 353–362.
He, C., L. Luo, Q.-M. Hao, and Y. Zhou (2013), Velocity-weakening behavior of plagioclase and pyroxene gouges and stabilizing effect of small amounts of quartz under hydrothermal conditions, *J. Geophys. Res. Solid Earth*, *118*, 3408–3430, doi:10.1002/jgrb.50280.
Heslot, F., T. Baumberger, B. Perrin, and C. Caroli (1994), Creep, Stick-slip, and dry-friction dynamics: Experiments and a heuristic model, *Phys. Rev. E*, *49*(6), 4973–4988.
Hill, D. P., P. Mowinckel, and K. M. Lahr (1975), Catalog of earthquakes in the Imperial Valley, California, June 1973-May 1974, Report number: 75-401, technical report, U.S. Geol. Surv.
Hirose, H., K. Hirahara, F. Kimata, N. Fujii, and S. Miyazaki (1999), A slow thrust slip event following the two 1996 Hyuganada Earthquakes beneath the Bungo Channel, southwest Japan, *Geophys. Res. Lett.*, *26*(21), 3237–3240, doi:10.1029/1999GL010999.
Hirose, T., and T. Shimamoto (2005), Growth of molten zone as a mechanism of slip weakening of simulated faults in gabbro during frictional melting, *J. Geophys. Res.*, *110*, B05202, doi:10.1029/2004JB003207.
Hyndman, R., and K. Wang (1993), Thermal constraints on the zone of major thrust earthquake failure: The Cascadia subduction zone, *J. Geophys. Res.*, *98*(B2), 2039–2060.
Ikari, M. J., D. M. Saffer, and C. Marone (2009), Frictional and hydrologic properties of clay-rich fault gouge, *J. Geophys. Res.*, *114*, B05409, doi:10.1029/2008JB006089.
Ito, Y., K. Obara, K. Shiomi, S. Sekine, and H. Hirose (2007), Slow earthquakes coincident with episodic tremors and slow slip events, *Science*, *315*(5811), 503–506, doi:10.1126/science.1134454.
Jackson, J. (2002), Strength of the continental lithosphere: Time to abandon the jelly sandwich?, *GSA Today*, *12*(9), 4–9.
Kaneko, Y., N. Lapusta, and J.-P. Ampuero (2008), Spectral element modeling of spontaneous earthquake rupture on rate and state faults: Effect of velocity-strengthening friction at shallow depths, *J. Geophys. Res.*, *113*, B09317, doi:10.1029/2007JB005553.
Kaproth, B. M., and C. Marone (2013), Slow earthquakes, preseismic velocity changes, and the origin of slow frictional stick-slip, *Science*, *341*(6151), 1229–1232.
Kato, N., and T. E. Tullis (2001), A composite rate-and state-dependent law for rock friction, *Geophys. Res. Lett.*, *28*(6), 1103–1106.
Keefner, J., S. Mackwell, D. Kohlstedt, and F. Heidelbach (2011), Dependence of dislocation creep of dunite on oxygen fugacity: Implications for viscosity variations in Earth's mantle, *J. Geophys. Res.*, *116*, B05201, doi:10.1029/2010JB007748.
Kimura, G., and A. Mukai (1991), Underplated units in an accretionary complex: Melange of the Shimanto Belt of eastern Shikoku, southwest Japan, *Tectonics*, *10*(1), 31–50.
King, D., and C. Marone (2012), Frictional properties of olivine at high temperature with applications to the strength and dynamics of the oceanic lithosphere, *J. Geophys. Res.*, *117*, B12203, doi:10.1029/2012JB009511.
Kodaira, S., T. Iidaka, A. Kato, J.-O. Park, T. Iwasaki, and Y. Kaneda (2004), High pore fluid pressure may cause silent slip in the Nankai Trough, *Science*, *304*(5675), 1295–1298.
Leyton, F., A. Pérez, J. Campos, R. Rauld, and E. Kausel (2009), Anomalous seismicity in the lower crust of the Santiago Basin, Chile, *Phys. Earth Planet. Inter.*, *175*(1), 17–25.
Linde, A. T., M. T. Gladwin, M. J. Johnston, R. L. Gwyther, and R. G. Bilham (1996), A slow earthquake sequence on the San Andreas fault, *Nature*, *383*(6595), 65–68.
Liu, Y., and J. R. Rice (2005), Aseismic slip transients emerge spontaneously in three-dimensional rate and state modeling of subduction earthquake sequences, *J. Geophys. Res.*, *110*, B08307, doi:10.1029/2004JB003424.
Liu, Y., and J. R. Rice (2009), Slow slip predictions based on granite and gabbro friction data compared to GPS measurements in northern Cascadia, *J. Geophys. Res.*, *114*, B09407, doi:10.1029/2008JB006142.
Liu, Y., J. J. McGuire, and M. D. Behn (2012), Frictional behavior of oceanic transform faults and its influence on earthquake characteristics, *J. Geophys. Res.*, *117*, B04315, doi:10.1029/2011JB009025.
Louie, J. N., C. R. Allen, D. C. Johnson, P. C. Haase, and S. N. Cohn (1985), Fault slip in southern California, *Bull. Seismol. Soc. Am.*, *75*(3), 811–833.
Malvoisin, B., F. Brunet, J. Carlut, S. Rouméjon, and M. Cannat (2012), Serpentinization of oceanic peridotites: 2. Kinetics and processes of San Carlos olivine hydrothermal alteration, *J. Geophys. Res.*, *117*, B04102, doi:10.1029/2011JB008842.
Marone, C. (1998), Laboratory-derived friction laws and their application to seismic faulting, *Annu. Rev. Earth Planet. Sci.*, *26*, 643–696.
Marone, C., and S. Cox (1994), Scaling of rock friction constitutive parameters: The effects of surface roughness and cumulative offset on friction of gabbro, *Pure Appl. Geophys.*, *143*(1-3), 359–385.
Matsubara, M., K. Obara, and K. Kasahara (2009), High-V_P/V_S zone accompanying non-volcanic tremors and slow-slip events beneath southwestern Japan, *Tectonophysics*, *472*(1–4), 6–17, doi:10.1016/j.tecto.2008.06.013.

McKenzie, D., J. Jackson, and K. Priestley (2005), Thermal structure of oceanic and continental lithosphere, *Earth Planet. Sci. Lett.*, *233*(3-4), 337–349, doi:10.1016/j.epsl.2005.02.005.
Mei, S., and D. Kohlstedt (2000a), Influence of water on plastic deformation of olivine aggregates: 1. Diffusion creep regime, *J. Geophys. Res.*, *105*(B9), 21,457–21,469.
Mei, S., and D. Kohlstedt (2000b), Influence of water on plastic deformation of olivine aggregates: 2. Dislocation creep regime, *J. Geophys. Res.*, *105*(B9), 21,471–21,481.
Mitchell, E., Y. Fialko, and K. Brown (2013), Temperature dependence of frictional healing of Westerly granite: Experimental observations and numerical simulations, *Geochem. Geophys. Geosyst.*, *14*, 567–582, doi:10.1029/2012GC004241.
Moore, J. C., and D. Saffer (2001), Updip limit of the seismogenic zone beneath the accretionary prism of southwest Japan: An effect of diagenetic to low-grade metamorphic processes and increasing effective stress, *Geology*, *29*(2), 183–186.
Nagata, K., M. Nakatani, and S. Yoshida (2012), A revised rate- and state-dependent friction law obtained by constraining constitutive and evolution laws separately with laboratory data, *J. Geophys. Res.*, *117*, B02314, doi:10.1029/2011JB008818.
Nakatani, M. (2001), Conceptual and physical clarification of rate and state friction: Frictional sliding as a thermally activated rheology, *J. Geophys. Res.*, *106*(B7), 13,347–13,380.
Niemeijer, A., G. Di Toro, S. Nielsen, and F. Di Felice (2011), Frictional melting of gabbro under extreme experimental conditions of normal stress, acceleration, and sliding velocity, *J. Geophys. Res.*, *116*, B07404, doi:10.1029/2010JB008181.
Obara, K. (2002), Nonvolcanic deep tremor associated with subduction in southwest Japan, *Science*, *296*(5573), 1679–1681.
Obara, K., and H. Hirose (2006), Non-volcanic deep low-frequency tremors accompanying slow slips in the southwest Japan subduction zone, *Tectonophysics*, *417*(1–2), 33–51, doi:10.1016/j.tecto.2005.04.013.
Obara, K., H. Hirose, F. Yamamizu, and K. Kasahara (2004), Episodic slow slip events accompanied by non-volcanic tremors in southwest Japan subduction zone, *Geophys. Res. Lett.*, *31*, L23602, doi:10.1029/2004GL020848.
Peng, Z., and J. Gomberg (2010), An integrated perspective of the continuum between earthquakes and slow-slip phenomena, *Nat. Geosci.*, *3*(9), 599–607.
Perfettini, H., and J.-P. Ampuero (2008), Dynamics of a velocity strengthening fault region: Implications for slow earthquakes and postseismic slip, *J. Geophys. Res.*, *113*, B09411, doi:10.1029/2007JB005398.
Plank, T., and C. H. Langmuir (1998), The chemical composition of subducting sediment and its consequences for the crust and mantle, *Chem. Geol.*, *145*(3), 325–394.
Rogers, G., and H. Dragert (2003), Episodic tremor and slip on the cascadia subduction zone: The chatter of silent slip, *Science*, *300*(5627), 1942–1943, doi:10.1126/science.1084783.
Rubin, A. M. (2008), Episodic slow slip events and rate-and-state friction, *J. Geophys. Res.*, *113*, B11414, doi:10.1029/2008JB005642.
Rubinstein, J. L., J. E. Vidale, J. Gomberg, P. Bodin, K. C. Creager, and S. D. Malone (2007), Non-volcanic tremor driven by large transient shear stresses, *Nature*, *448*(7153), 579–582.
Ruina, A. (1983), Slip instability and state variable friction laws, *J. Geophys. Res.*, *88*(10), 10,359–10,370.
Saffer, D. M., and C. Marone (2003), Comparison of smectite-and illite-rich gouge frictional properties: Application to the updip limit of the seismogenic zone along subduction megathrusts, *Earth Planet. Sci. Lett.*, *215*(1), 219–235.
Saffer, D. M., and L. M. Wallace (2015), The frictional, hydrologic, metamorphic and thermal habitat of shallow slow earthquakes, *Nat. Geosci.*, *8*, 594–600.
Schleicher, A., B. van der Pluijm, and L. Warr (2012), Chlorite-smectite clay minerals and fault behavior: New evidence from the San Andreas Fault Observatory at Depth (SAFOD) core, *Lithosphere*, *4*(3), 209–220.
Schwartz, S. Y., and J. M. Rokosky (2007), Slow slip events and seismic tremor at circum-Pacific subduction zones, *Rev. Geophys.*, *45*, RG3004, doi:10.1029/2006RG000208.
Segall, P., A. M. Rubin, A. M. Bradley, and J. R. Rice (2010), Dilatant strengthening as a mechanism for slow slip events, *J. Geophys. Res.*, *115*, B12305, doi:10.1029/2010JB007449.
Sibson, R. H. (1982), Fault zone models, heat flow, and the depth distribution of earthquakes in the continental crust of the United States, *Bull. Seismol. Soc. Am.*, *72*(1), 151–163.
Sleep, N. H. (1997), Application of a unified rate and state friction theory to the mechanics of fault zones with strain localization, *J. Geophys. Res.*, *102*(B2), 2875–2895.
Stesky, R., W. Brace, D. Riley, and P.-Y. Robin (1974), Friction in faulted rock at high temperature and pressure, *Tectonophysics*, *23*(1), 177–203.
Tichelaar, B. W., and L. J. Ruff (1993), Depth of seismic coupling along subduction zones, *J. Geophys. Res.*, *98*(B2), 2017–2037.
Tse, S. T., and J. R. Rice (1986), Crustal earthquake instability in relation to the depth variation of frictional slip properties, *J. Geophys. Res.*, *91*(B9), 9452–9472.
Wei, M., D. Sandwell, and Y. Fialko (2009), A silent Mw 4.7 slip event of October 2006 on the Superstition Hills fault, southern California, *J. Geophys. Res.*, *114*, B07402, doi:10.1029/2008JB006135.
Wesson, R. L., R. O. Burford, and W. L. Ellsworth (1973), Relationship between seismicity, fault creep and crustal loading along the central San Andreas fault, in *Proceedings of the Conference on Tectonic Problems of the San Andreas Fault System*, Stanford University, Stanford, Calif., vol. 13, pp. 303–321.